New Developments with C–Mn–Ni High Strength Steel Weld Metals — Part A. Microstructure

E. Keehan*, M. Murugananth**+, L. Karlsson***,
H.-O. Andrén* and H. K. D. H. Bhadeshia**

* Department of Experimental Physics, Chalmers University of Technology,
SE – 412 96 Gothenburg, Sweden.

**University of Cambridge, Department of Materials Science and Metallurgy,
Pembroke Street, Cambridge CB2 3QZ, U.K.

***ESAB AB, P.O. Box 8004, SE – 402 77 Gothenburg, Sweden.

+ Presently at School of Materials Engineering,
Nanyang Technological University, Singapore 639 798.

Abstract

The relationship between alloying content, microstructure and properties has been studied for high strength steel weld metals with 7 to 9 wt. % nickel. Neural network modelling suggested that manganese reductions lead to large impact toughness increases and that nickel must be added in a controlled manner with respect to manganese in order toincrease impact toughness. Carbon additions were predicted to enhance yield strength at limited loss to impact toughness. Following these predictions, shielded metal arc welding was used to produce experimental welds with manganese at 0.5 or 2 wt. %, nickel at 7 or 9 wt. % while carbon was varied between 0.03 and 0.11 wt. %. Based on Themo-Calc calculations and the observed segregation behaviour, it was concluded that the weld metals solidified completely as austenite. With high resolution microscopy the microstructure was found to be a mixture of predominantly upper bainite and a coarse grained, previously not documented, constituent characterised to be coalesced bainite in dendrite core regions, with mainly martensite present in interdendritic regions for high manganese weld metals. Manganese reductions were found to promote upper bainite while carbon additions were found to promote martensite. A constitutional diagram was constructed that summarises microstructure as a function of manganese and nickel contents. In Part B of this work, the mechanical properties are presented and discussed in relation to the microstructure and the neural network predictions .

Background

Steels with yield strengths in the region of 1000 MPa that possess good impact toughness have been readily available for some time. They are increasingly employed in many applications

offering both size and weight reduction. In many applications, it is an engineering requirement that a weld metal with matching or overmatching strength is used in the joining. It is well known that maintaining good toughness becomes more problematic as strength levels increase above the region of 690 MPa (100 ksi) with the more flexible and productive welding methods such as shielded metal arc welding (SMAW), flux cored arc welding (FCAW) or submerged arc welding (SAW) [1, 2]. As a result there is a need to develop new high strength welding consumables that meet the market requirements.

Metallurgists have addressed the challenges of increasing strength and toughness in steel through grain refinement, precipitation hardening, solid solution hardening, thermomechanical treatment and the promotion of low temperature transformations products such as martensite and bainite [3]. Carbon additions have a great strengthening effect on iron and when combined with alloying elements such as manganese, nickel and chromium very high strengths are attainable. Elements such as Ni and Mn are commonly added to weld metals in order to increase strength and toughness. These elements are not carbide formers and instead provide solid solution hardening. Both also reduce the austenite to ferrite transformation temperature and Ni is reported to influence the stacking fault energy of ferrite at low temperatures in such manner that plastic deformation is accommodated [4–6].

Up to now, many have kept the above theories in mind and carried out research by varying elemental composition or welding parameters with the aim of optimising weld metal properties. High strength steel weld metals have usually C less than 0.2 wt. %, Ni less than 4 wt. % and Mn less than 4 wt. % [1, 7–22]. Results generated yield strengths ranging from below 500 MPa to above 1000 MPa. However, with the common flux shielded welding processes, good impact toughness was mostly achieved at lower yield strengths.

For example, the promising work by Lord [14] used the composition of a commercial SMAW consumable (ESAB OK 75.78 with 3 Ni, 2 Mn, 0.5 Cr, 0.6 Mo, 0.05 C) as the basis of development. He increased nickel concentrations to 4 wt. % at decreasing Mn levels between 1.1 and 0.8 wt. %. It was found that impact toughness increased to 74 J at –60 ºC and the yield strength was reduced to 809 MPa [14]. Kang followed the trend of increasing Ni and reducing Mn with metal cored wires. He recorded an impact toughness of 55 J at –60 °C with Ni at 6.95 wt. % and Mn at 0.52 wt. %. Tensile strength of 684 MPa was predicted for this alloy from hardness results. With microstructural investigations, the presence of lath martensite and various forms of ferrite was confirmed [23]. In previous work it is generally found that as impact toughness increases, yield and tensile strength decrease. To limit strength losses, carbon additions and reducing interpass temperature have been most effective [24–25]. For example carbon levels up to 0.08 wt. % combined with 2–4 Ni and 1.4–2.0 Mn were found good for strength with limited losses in impact toughness [24]. In another study it was found that yield and ultimate tensile strength also increased with decrease in interpass temperature [25]. In both cases, changes in

mechanical properties were claimed to be strongly related to the microstructure described as mixtures of martensite and bainite.

With Lord's work [14] as our starting point, neural network modelling was engaged to optimise the development process and to allow the effects of a wide variety of parameters to be perceived. The technique and the advantages it offers materials science are further described in [26–28]. A brief description of the modelling applied in this research is given here and more complete details may be found in [29–30]. The present report is Part A of two reporting on work carried out on high strength steel weld metals with variations in nickel, manganese and carbon. Using SMAW, the effects were studied of varying nickel at 7 or 9 wt %, manganese at 0.5 or 2.0 wt. % and carbon between 0.03 and 0.11 wt. % on the microstructure (Part A) and the mechanical properties (Part B [31]).

Neural Network Modelling

Four neural network models were constructed to predict impact toughness, yield strength (YS), ultimate tensile strength (UTS) and elongation based on a database of some 3300 experimental weld metal results. An assessment was made for the optimum size of committee for each mechanical property since it is frequently found that a committee of models can give better predictions [26–27]. The results of the assessment are presented in Table 1.

Using the base composition presented in Table 2 along with an energy input of 1 kJ / mm and an interpass temperature of 250 ºC, a contour plot was generated for impact toughness behaviour at –60 ºC for varied manganese and nickel. The predictions are surprising in that manganese reductions at all nickel levels lead to impact toughness increases. The contour plots also suggest that below a certain critical concentration of manganese, controlled additions of nickel can

Model	No. of members in committee	σ_v (Max Percieved Noise)
Impact Toughness / J	5	0.083
YS / MPa	13	0.04
UTS / MPa	5	0.023
Elongation / %	2	0.064

Table 1 Some basic neural network model characteristics.

Element	Content
C	0.034
Cr	0.5
Si	0.25
P	0.01
Mo	0.62
V	0.011
Cu	0.04
Co	0.009
W	0.005
S / ppm	0.008
B / ppm	1
Ti / ppm	80
Nb / ppm	10
O / ppm	380
N / ppm	250

Table 2 The base composition used for analysing the effects of nickel and manganese concentration in neural network modelling. All elements are in wt. %. unless otherwise stated.

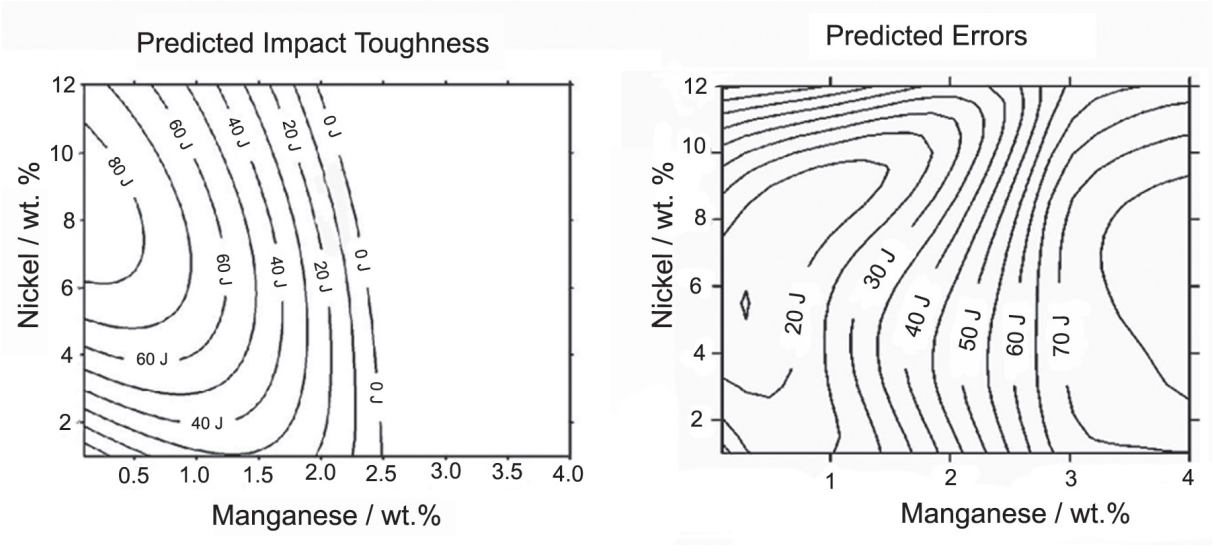

Figure 1 Contour plots showing the calculated weld metal impact toughness at –60 ºC as a function of manganese and nickel concentrations. The errors represent ± 1 σ of uncertainty.

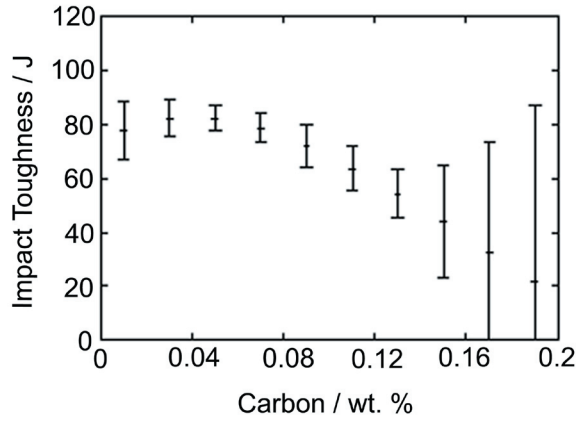

Figure 2 Predicted impact toughness at –60 ºC as a function of carbon concentration. The error bars represent ± 1 σ of uncertainty.

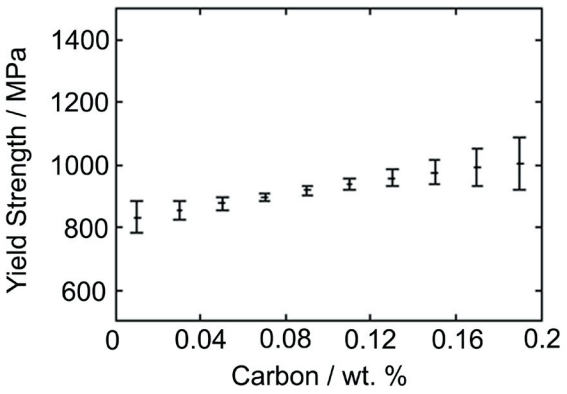

Figure 3 Predicted yield strength as a function of carbon concentration. The error bars represent ± 1 σ of uncertainty.

lead to an increase in impact toughness as well as strength. However, the reverse mechanical behaviour was predicted if nickel exceeds critical levels depending on the manganese concentration.

Given that the contour plot suggested the best impact toughness would be achieved with Mn and Ni concentrations in the region of 0.5 wt. % and 7.0 wt. %, respectively, the base input composition for further calculations was set at these values. Since it is well known that additions of carbon lead to strength increases, it was estimated with the models how yield strength and impact toughness would behave with carbon variations between 0 and 0.2 wt. %. The results of these predictions are presented in Figures 2 and 3. It is shown that yield strength is predicted to increase from the region of 830 MPa to just slightly over 1000 MPa when the carbon content is

increase from 0.01 wt. % C to 0.19 wt. %. It was noted that impact toughness levels at –60 ºC are predicted to remain acceptable with carbon additions up to the region of 0.12 wt. %. Above this content, there are insufficient data to predict accurately as shown by large error bars.

Experimental Techniques

Based primarily on the neural network predictions, seven experimental weld metals were produced using SMAW. It was decided to study the changes in mechanical and microstructural behaviour in detail for Mn concentrations of 0.5 or 2.0 wt. %, Ni levels at 7 or 9 wt. % and carbon additions from 0.03 to 0.11 wt % with Ni at 7 wt. % and Mn at 0.5 wt. %.

Welded joints were made according to ISO 2560 using 20 mm plates with a backing plate. The joints were buttered prior to the deposition of the experimental weld metals that took place in 33 cm runs with two or three runs per layer. The energy input and interpass temperature are presented in Table 3. Names were assigned to the weld metals according to composition and interpass temperature. 7 or 9 is the Ni content, 2 or 0.5 is the Mn content, L, M or H are the low, medium, or high carbon contents and 200 or 250 is the interpass temperatures. The estimated cooling time between 800 and 500 ºC ($t_{8/5}$) was calculated using the WeldCalc program [32]. Samples of weld metal were analysed using a Spectro Lab S optical emission spectrometer and Leco combustion equipment (Model EF500 for C and S and model TC – 436 DR for N and O). The compositions of the weld metals are presented in Table 3.

Weld Metal	7-2L250	9-2L250	7-0.5L250	7-0.5L200	9-0.5L200	7-0.5M200	7-0.5H200
E / kJ mm^{-1}	1.2	1.2	1.0	1.3	0.7	1.4	1.3
IPT / °C	250	250	250	200	200	200	200
$t_{8/5}$ / s	12	11	10	10	5	11	10
C *	0.032	0.031	0.024	0.030	0.026	0.061	0.110
Mn	2.02	2.11	0.64	0.61	0.37	0.56	0.53
Ni	7.23	9.23	6.6	6.11	8.67	6.84	7.04
Cr	0.47	0.48	0.21	0.16	0.2	0.15	0.14
Si	0.25	0.27	0.35	0.4	0.34	0.34	0.38
S*	0.008	0.008	0.008	0.009	0.008	0.006	0.007
P	0.011	0.011	0.012	0.010	0.007	0.011	0.008
Mo	0.63	0.64	0.4	0.38	0.41	0.35	0.40
V	n.a.	n.a.	n.a.	0.018	n.a	0.014	0.016
Cu	0.03	0.03	0.03	0.02	0.01	0.01	n.a
O / ppm *	380	340	400	340	367	350	260
N / ppm *	250	260	197	150	130	160	100

Table 3 Welding parameters and chemical composition. Welding parameters presented are energy input (E), interpass temperature (IPT) and the estimated cooling time between 800 and 500 °C ($t_{8/5}$) calculated from WeldCalc [32]. Composition is in wt. % unless otherwise stated, '*' indicate elements analysed using Leco Combustion equipment and "n.a." are elements not analysed.

Specimens from the weld metal cross section, extracted perpendicular to the welding direction were mounted in bakelite, wet ground, polished to 1 μm and etched using 2 % nital etchant for analysis with LOM and field emission gun scanning electron microscopy (FEGSEM). A Leitz Aristomet light optical microscope and a Leo Ultra 55 FEGSEM were used in these examinations. Polished specimens were examined with scanning electron microscopy (SEM) in the back scattered mode and elemental analysis was carried out using Energy Dispersive X-ray analysis (EDX). For TEM studies, 3 mm disc shape samples, perpendicular to the welding direction, were ground to between 50 and 80 μm in thickness and then jet electropolished at –35 °C using 10 % perchloric acid in methanol. After electropolishing the specimens were further thinned by ion beam milling for a few minutes at a low angle using a Gatan Precision Ion Polishing System (PIPS). These specimens were examined with a Jeol 2000 FX or a Philips CM200 TEM.

Dilatometer specimens in the form of cylinders with a diameter of 3 mm and a length of 10 mm were machined from the centre of the welded joint. These were then investigated using a Theta Dilatronic III dilatometer. The specimens were heated to 1000 °C at a rate of 25 °C / s, held for 5 minutes and afterwards cooled to room temperature at different cooling rates. Individual samples were used for each cooling rate.

Results

Microstructure – The last bead

The welded joints comprised different regions and the microstructure of the joint was inhomogeneous from region to region – typical of a normal welded joint. The last bead of each weld was found to consist of a columnar structure with the columns varying in size but normally less

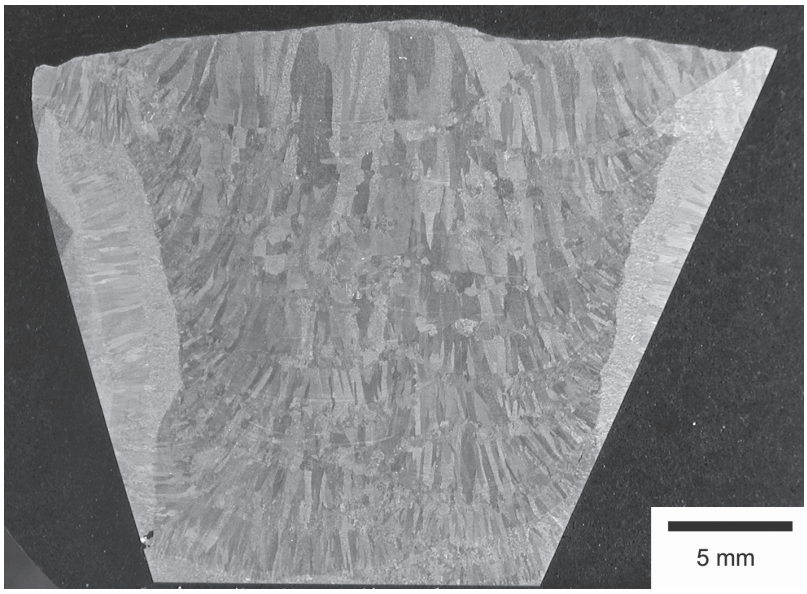

Figure 4 A low magnification light optical micrograph from 7-2L250 showing a cross section of the welded joint.

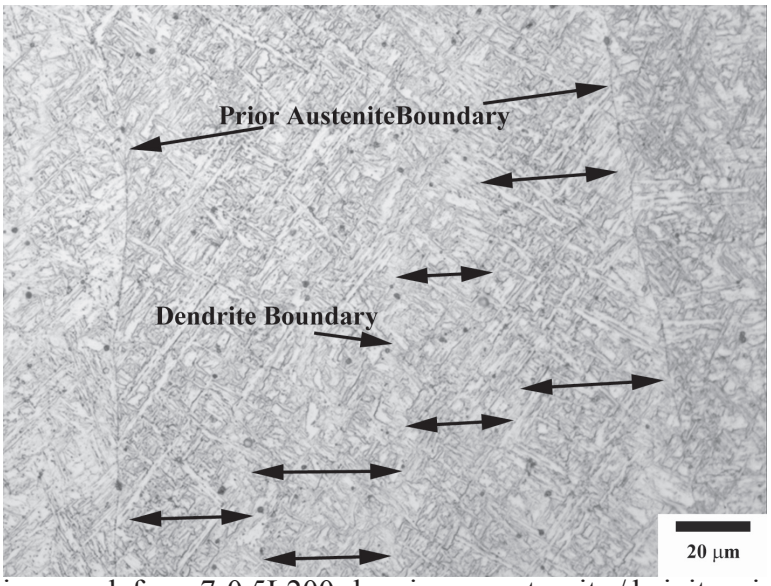

Figure 5 LOM micrograph from 7-0.5L200 showing a martensite / bainite microstructure. Here it is seen that dendrites formed within the columnar structure as the weld metal solidified.

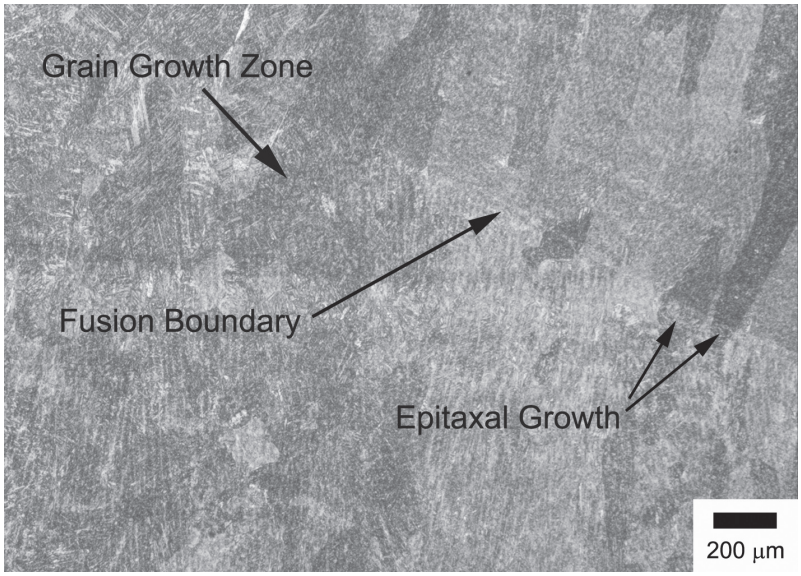

Figure 6 Light optical micrograph from 7-0.5L200 showing the fusion zone between the last bead and underlying weld metal. Epitaxal growth between the beads and a grain growth zone in the underlying weld metal is clearly seen.

than 0.5 mm in width (Figure 4). These columns were further subdivided into a cellular structure of dendrites with a thickness between 10 and 30 μm (Figure 5). A fine scale microstructure typical of bainite or martensite was formed within the dendrites. Figure 6 shows the fusion zone between the last bead and underlying beads in 7-0.5L200. The fusion boundary is easily recognised and it is seen that solidification began as a result of epitaxial growth between the beads. A small amount of grain growth was observed just below the last bead.

Figures 7 and 8 present the variation of microstructure in the as-deposited last bead as a result of changing nickel, and carbon content. In the images the former dendrite boundaries can be seen.

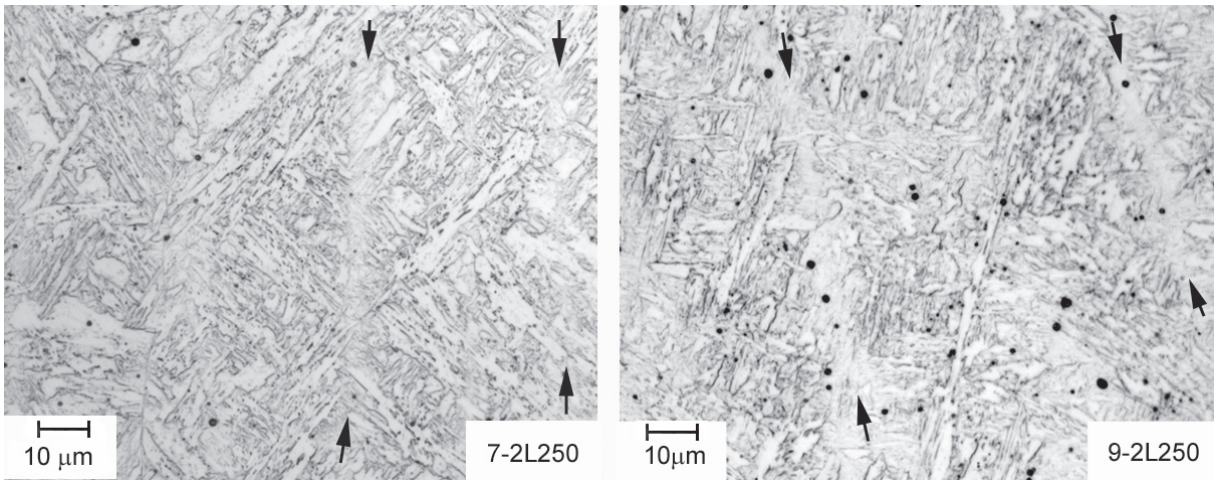

Figure 7 LOM micrographs of the as-deposited last bead from 7-2L250 and 9-2L250 showing a fine scale microstructure with large grains not typically found in high strength steel weld metals. The black arrows indicate the former dendrite boundaries.

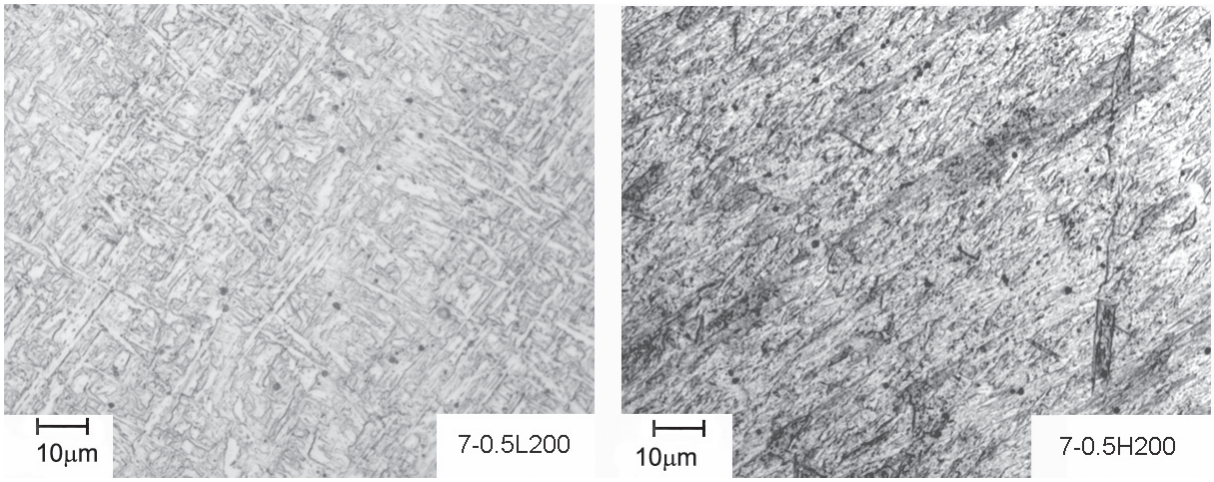

Figure 8 The refinement of the microstructure with increasing C content is clearly seen by comparing LOM micrographs of as-deposited last bead of 7-0.5L200 and 7-0.5H200.

The microstructure is very fine scale, typical of martensite or bainite, but it is not possible to decipher between the two with LOM due to their similar morphologies. Large grains not commonly found in high strength steel weld metals were also observed in particular with 7-2L250 and 9-2L250. LOM images from the as-deposited last bead in 7-0.5L200 and 7-0.5H200 are shown in Figure 8 which allows the effect of changing carbon from 0.03 wt. % to 0.11 wt. % to be observed. It was found that the microstructure becomes very fine with increase of carbon content but again it is not possible with LOM to identify the microstructure with full certainty and investigations with instruments offering better resolution are necessary. This work has been carried out and full details may be found elsewhere [33–36]. A summary is presented here.

The as-deposited last bead microstructure of weld metals 7-2L250, 7-0.5L250 and 7-0.5H200 is shown in Figure 9. Focusing on weld metal 7-2L250, it was investigated in great detail both

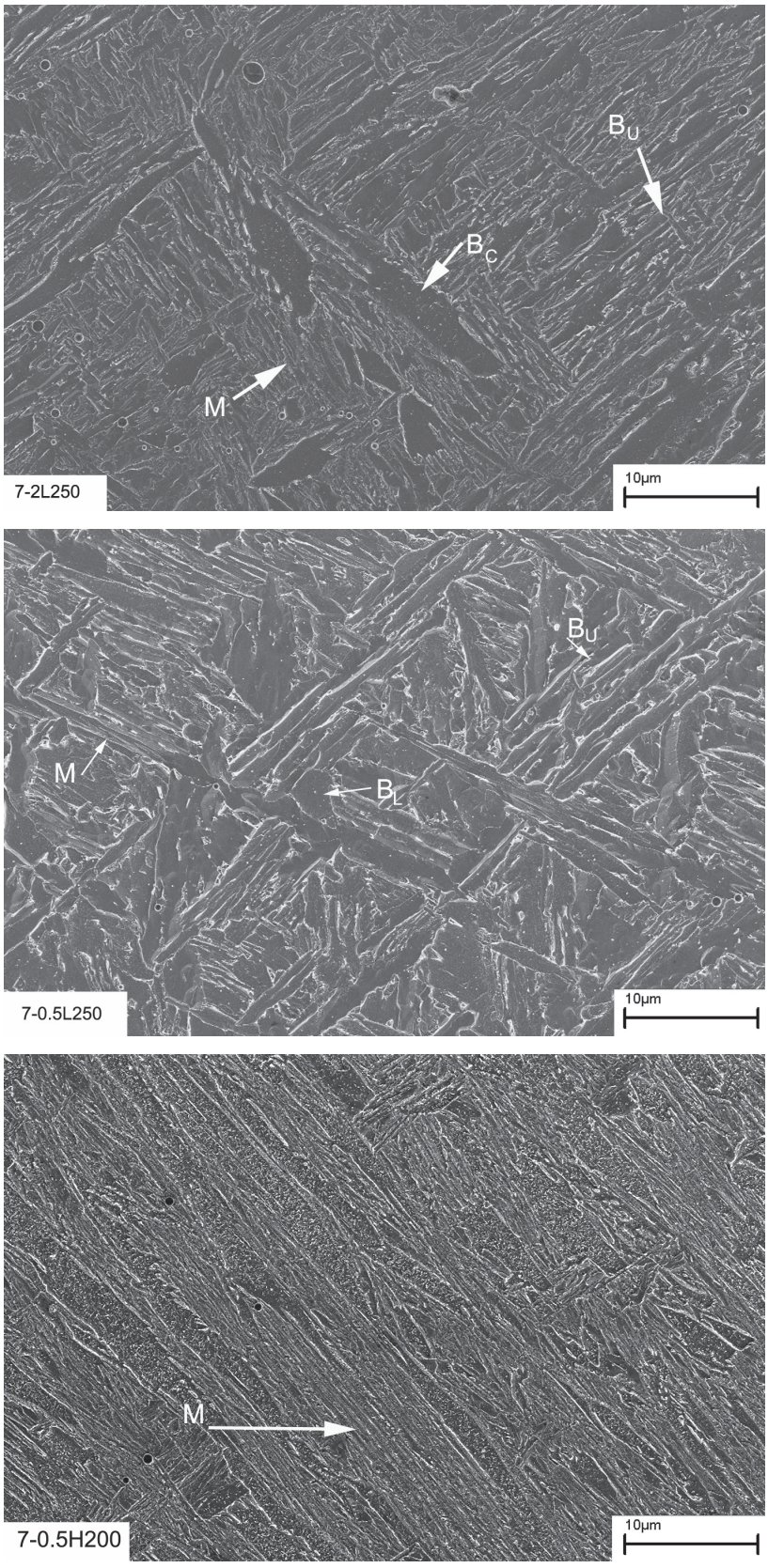

Figure 9 The microstructure in the as-deposited last bead of weld metals 7-2L250, 7-0.5L250 and 7-0.5H200 imaged using FEGSEM. M is for martensite, B_U is upper bainite, B_L is lower bainite and B_C is coalesced bainite.

with FEGSEM and TEM. The constituent with a large grain size, also seen with LOM in Figure 7, was characterised to be a previously not reported variant of bainite that forms through a coalescence of supersaturated bainitic ferrite plates when M_S and B_S are close. Full details of its characterisation are presented elsewhere [33]. A FEGSEM micrograph showing coalesced bainite at slightly higher magnification is presented in Figure 10. Using electron diffraction it was found that cementite precipitates formed within the bainitic ferrite grains (Figure 11). Generally the coalesced bainite was found along with upper bainite in dendrite core regions while a lath-like microstructure of martensite was found at interdendritic regions. An interdendritic region is shown at higher magnification in Figure 12 where the morphology of martensite can be seen. It is also observed that a small distance away from the interdendritic region upper bainite forms. Overall it was found that the microstructure in weld metal 9-2L250 was very similar to that of 7-2L250 with the same microstructural constituents developing [33].

Comparing the micrographs from 7-2L250 and 7-0.5L250 in Figure 9 the effects of reducing Mn content from 2 to 0.5 wt. % at nickel content of 7 wt. % may be observed. With 7-0.5L250 there was the noticeable absence of coalesced bainite and the microstructure was predominately upper and lower bainite in former dendrite core regions while martensite was the main constitu-

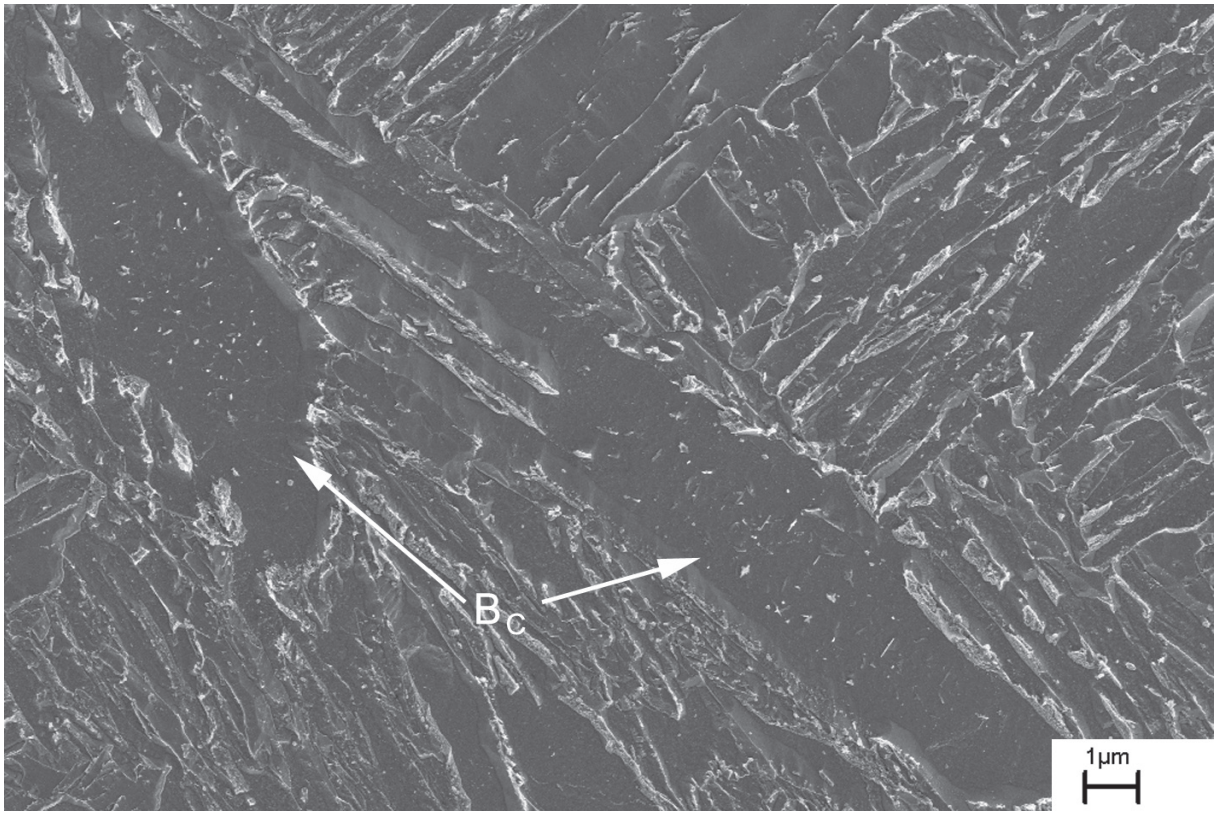

Figure 10 Coalesced bainite in weld metal 7-2L250. Small precipitates can be observed within the bainitic ferrite grains.

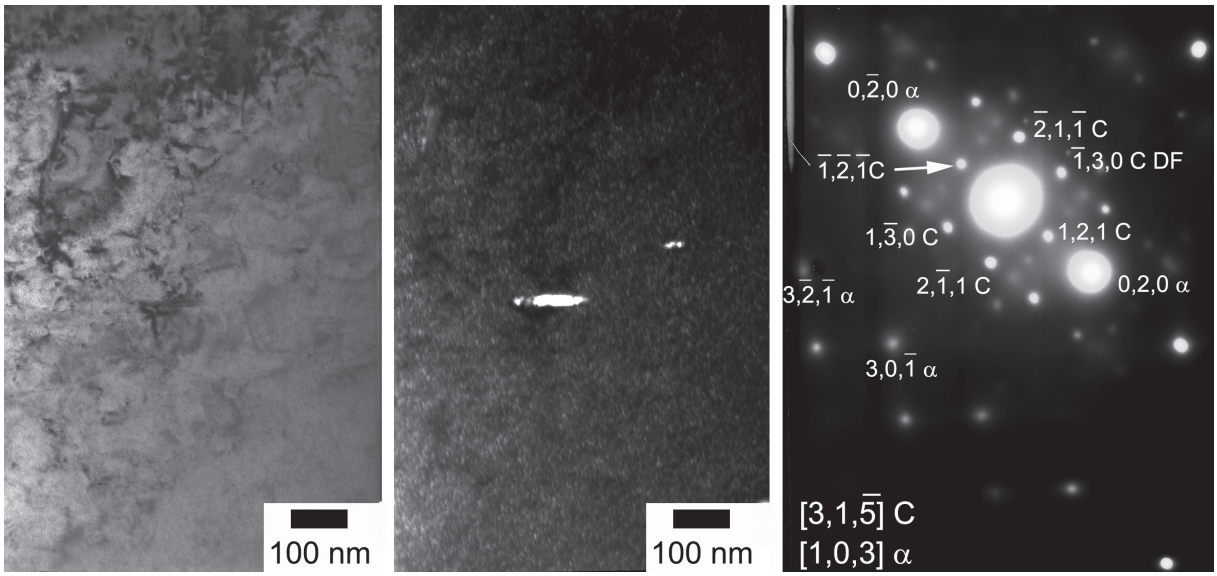

Figure 11 TEM bright (left) and dark (middle) field images with corresponding diffraction pattern (right) of a cementite precipitate within a coalesced bainitic ferrite grain. The dark field image was formed using the {–1,3,0} cementite reflection.

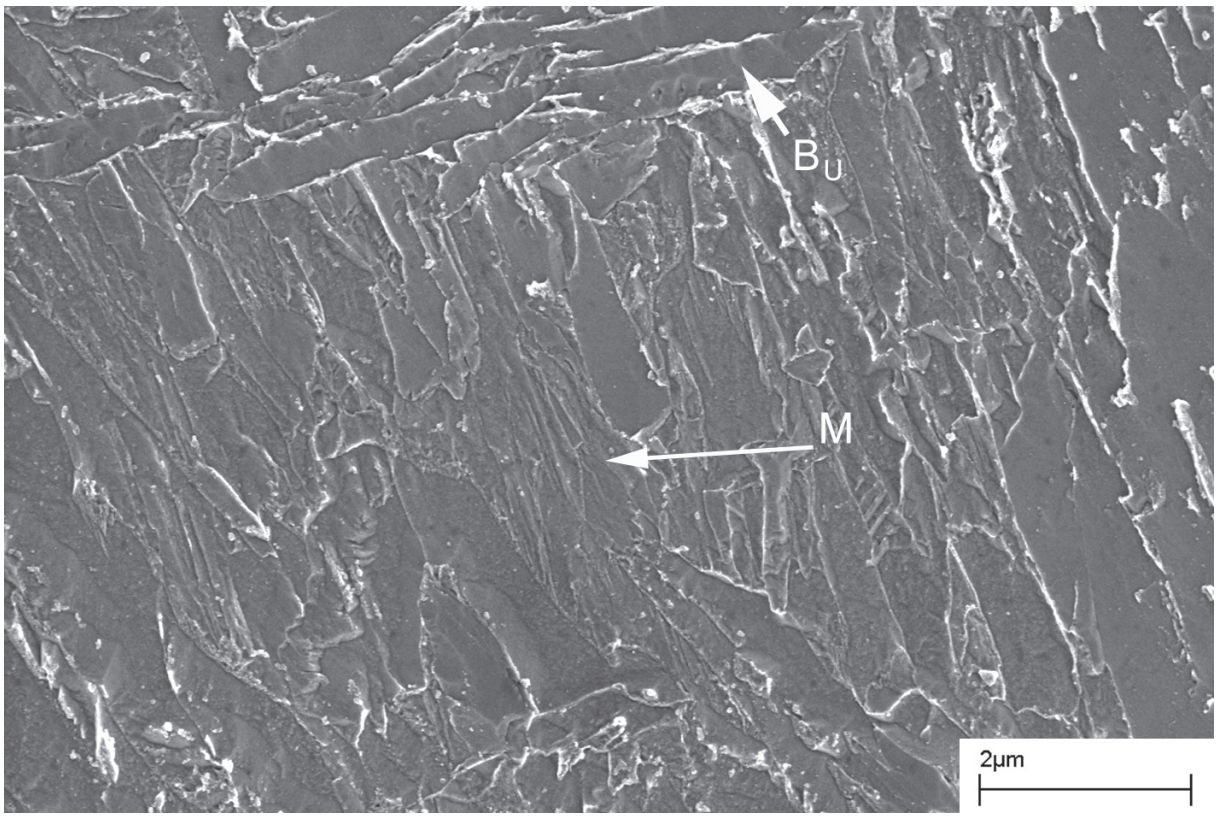

Figure 12 An interdendritic region in the last bead of weld metal 7-2L250 showing a mainly martensitic microstructure. M is martensite and B_U is upper bainite.

ent at interdendritic regions. It was found that carbon additions promote a finer microstructure with mainly martensite across the dendrites as shown with 7-0.5H200 (Figure 9) [36].

Elemental Segregation

When polished specimens from weld metals 7-2L250, 9-2L250 and 7-0.5L250 were examined in the backscattered mode, there was a clear contrast between the dendrite core regions and the interdendritic regions. This led to the observation that there may be significant elemental segregation across the former dendrites and it was decided to carry out EDX spot analysis. The results are presented in Table 4. In general it was found that manganese was overestimated in all analyses. Nevertheless, it was observed that interdendritic regions were enriched in nickel and manganese with weld metal 9-2L250 showing the greatest amounts of segregation.

Weld Metal	Mn		Ni
7-2L250 Boundary	3.1	(2.5)	8.18
7-2L250 Core	2.35	(1.75)	6.3
9-2L250 Boundary	3.2	(2.9)	10.3
9-2L250 Core	2.05	(1.75)	7.7
7-0.5L250 Boundary	0.95	(0.9)	7.55
7-0.5L250 Core	0.57	(0.5)	5.83

Table 4 Average compositions recorded in wt. % at dendritic boundary regions and dendrite core regions in the last bead using EDX spot analysis. Mn values in brackets are values adjusted using the average composition in Table 3 to allow for the overestimation of Mn with EDX.

Microstructure – Reheated beads

The microstructure in central beads was as expected even more complex which resulted from different thermal histories and tempering depending on the location within the joints. Figure 13 shows the centre of reheated beads in weld metals 7-0.5L200 and 7-0.5H200. From these images it is difficult to conclude what the microstructure is, but given the examinations in the last bead it is inferred to be that of mainly tempered bainite with 7-0.5L200 and mainly tempered martensite with 7-0.5H200.

An overview of the centre in a reheated bead in weld metal 7-0.5L250 is shown in Figure 14. Within the micrograph, the former dendrites are clearly seen. The same microstructural variation, as in the last bead, was found across the former dendrites except that it was tempered. In dendrite core regions, mainly tempered bainite (Figure 15) was found while tempered martensite (Figure 16) was predominantly found at interdendritic regions. In bainitic areas it was found that the carbon had redistributed within the bainitic ferrite. The cementite precipitates observed in the last bead (Figure 10) were found to have spheroidised within the grains

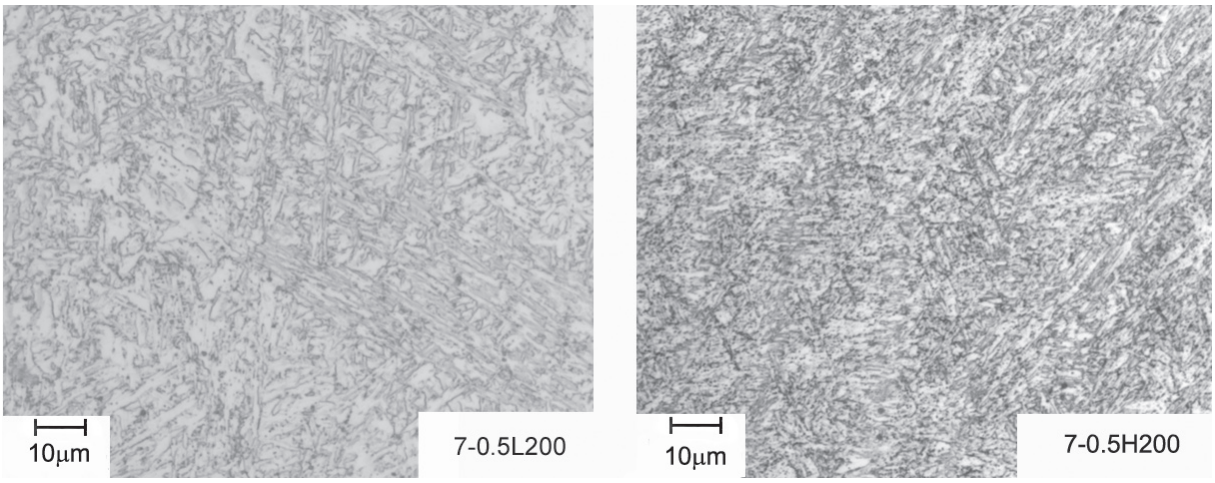

Figure 13 LOM micrographs from 7-0.5L200 and 7-0.5H200 showing the microstructure in the bead interior of reheated central beads in the joint.

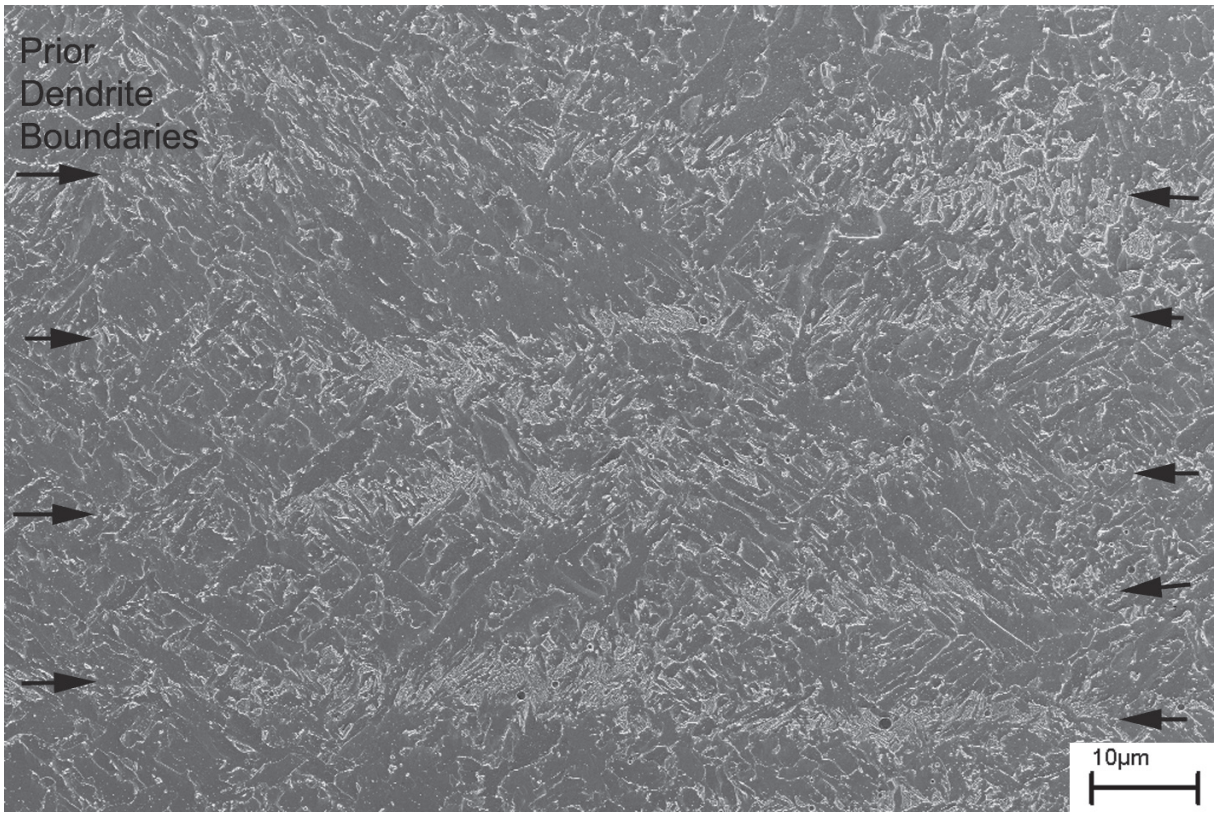

Figure 14 A FEGSEM overview of a reheated bead in weld metal 7-0.5L250.

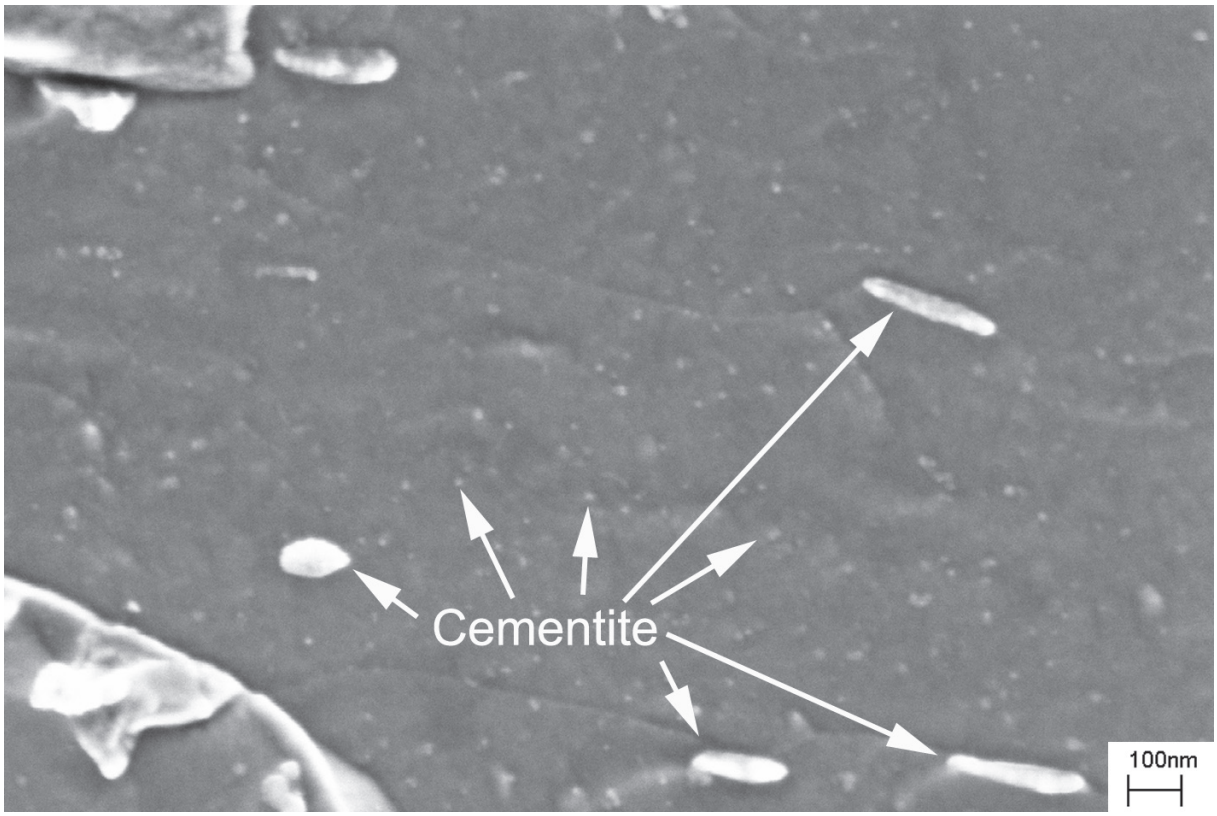

Figure 15 A high magnification FEGSEM micrograph showing spheroidised and coarsened cementite along with newly formed small precipitates in tempered bainite in a reheated bead of weld metal 7-2L250.

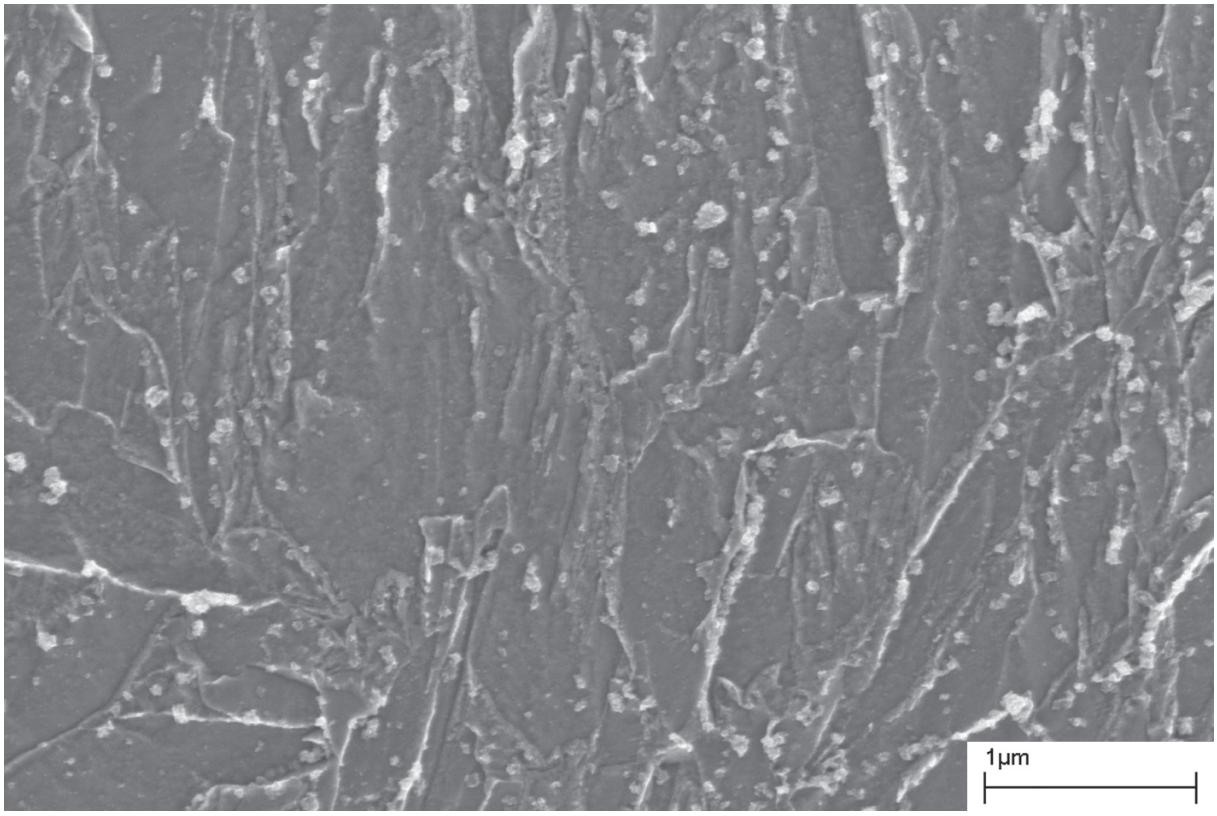

Figure 16 FEGSEM image of tempered martensite in a former interdendritic region within a reheated bead of weld metal 7-2L250.

and coarsened at the grain boundaries. In addition very small cementite precipitates in the order of a few nanometres had formed within the bainitic ferrite. These latter precipitates along with the former spheroidised and coarsened precipitates were confirmed to be cementite using TEM and electron diffraction [33–34].

Dilatometry

Transformation temperatures for the different weld metals are presented in Table 5. The results at cooling rates of 25–40 °C / s are representative of the cooling rates within the welded joints based on the $t_{8/5}$ calculations. Generally it can be said that greater alloying content with nickel, manganese and carbon stabilise austenite to lower temperatures. Overall there was no large difference in austenite transformation temperature as a result of changing the cooling rate.

It is seen by comparing 7-2L250 and 9-2L250 that nickel increases reduce both Ac_1 and Ac_3 temperatures and on cooling austenite is stabilised to lower temperatures. Comparing 7-2L250 and 7-0.5L250 it is found that a reduction in manganese content increases both Ac_1 and Ac_3

Weld Metal	Ac_1 / °C	Ac_3 / °C	Transformation of γ	
			25 – 40 °C / s cooling	1 °C / s cooling
7-2L250	690	740	373	390
9-2L250	665	720	365	365
7-0.5L250	700	770	490	480
7-0.5H200	685	770	355	365

Table 5 Austenite decomposition temperatures recorded using dilatometry.

temperatures and austenite transformation on cooling takes place in the region of 100 degrees higher. Carbon additions were found to reduce the Ac_1 temperature, but interestingly, Ac_3 was maintained at the same temperature as with low carbon levels. Austenite was stabilised to very low temperatures on cooling (365 °C), the same transformation temperature as with high nickel and manganese.

Thermo-Calc Calculations

Given that it is difficult to observe with microstructural studies whether the weld metals solidified as ferrite or austenite it was decided to use Thermo-Calc [37] to simulate the transformation based on alloying content. It was felt that the solidification mode is of particular importance for the final chemical distribution and knowledge was necessary to have a complete understanding of the final microstructure.

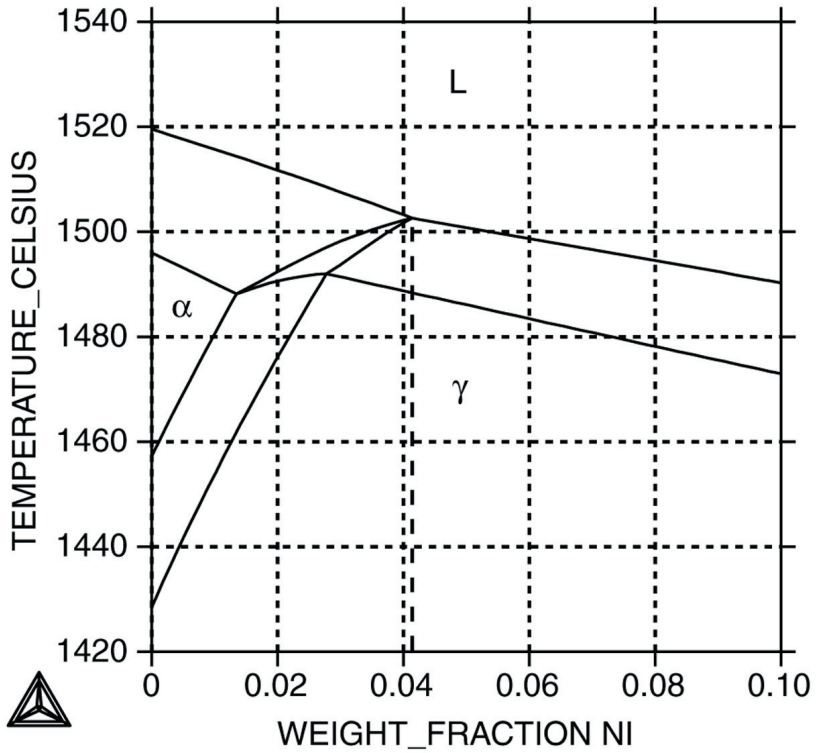

Figure 17 Isopleth as a function of nickel content and temperature based on the composition of weld metal 7-2L250 calculated using Thermo-Calc.

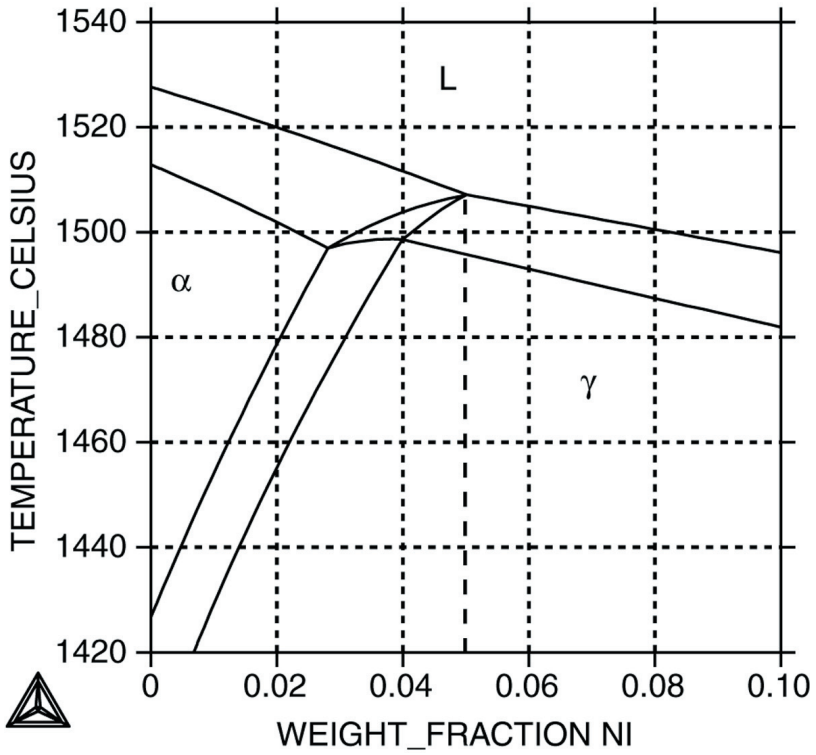

Figure 18 Isopleth calculated with Thermo-Calc for the composition of weld metal 7-0.5L250 as a function of nickel content and temperature.

Predictions from Thermo-Calc were made using the CCTSS database and are presented in Figures 17 to 19. The liquid to solid transformation as a function of nickel content and temperature for the base compositions of weld metals 7-2L250 and 7-0.5L250 are presented as isopleths in Figures 17 and 18, respectively. It is seen from the diagrams that ferrite can form during solidification at higher nickel contents with the lower manganese content. However even with 0.5 wt. % manganese, it is observed that at all nickel contents in the weld metals presented in Table 3 fully austenitic solidification will take place.

Figure 19 presents Scheil simulations for 7-0.5L250. In these calculations it is assumed that no diffusion occurs in the solid state after solidification and that the liquid is fully in equilibrium. In diagram (a) the weight fraction of solid is predicted as a function of temperature. In (b) the manganese content in wt. % as a function of the weight fraction solid is predicted while in (c) the nickel content in wt. % as a function of the weight fraction solid is shown.

Discussion

Solidification and Segregation

From Thermo-Calc simulations it was suggested that all the experimental weld metals solidified completely as austenite. Solidification as austenite may explain why the former dendritic structure is so clearly visible within the microstructure. Once solidification has taken place, diffusion of substitutional elements is much more limited in the austenitic lattice than in the ferrite lattice. The local chemistry at high temperatures is therefore inherited down to lower temperatures and thus may affect low temperature phase transformations.

An interesting comparison to make is between the Scheil simulations presented in Figure 19 and the EDX spot analysis results presented in Table 4. From the Scheil calculations for the weld metal 7-0.5L250 composition, it is predicted that the first solid to form has 0.45 wt. % Mn and 5.8 wt. % nickel (dendrite core regions) while the final composition to solidify is estimated to be 1.5 wt. % Mn and 10.2 wt. % Ni (interdendritic regions). Comparing these figures with EDX results, the average Mn and Ni content of the first solid to form was 0.57 and 5.83 wt. %, respectively, (dendrite core region) and the last solid to form had 0.95 wt. % Mn and 7.55 wt. % Ni. From this comparison, it is seen that there is fairly good agreement between the simulations and the actual measured alloying content considering the spatial resolution of EDX analysis and the fact that some diffusion will take place. Similar agreement was found for alloys 7-2L250 and 9-2L250 supporting the conclusion that the weld metals solidified as austenite.

Given that a greater alloying content is found at interdendritic regions, phase transformations and the final microstructure will be affected. With knowledge of the effects of alloying content, the variation in microstructure both across the dendrites and between the alloys can be understood and justified as will be discussed in the following section.

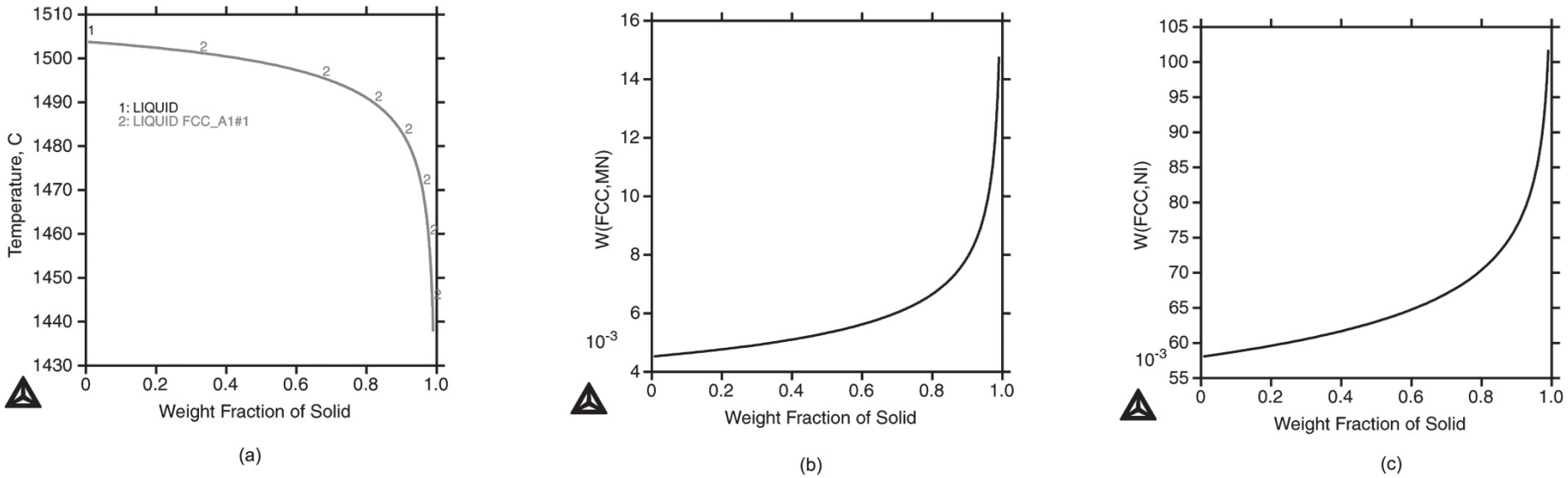

Figure 19 Scheil simulations for weld metal 7-0.5L250 of (a) the weight fraction of solid as a function of temperature, (b) manganese content as a function of the weight fraction of solid and (c) nickel content as a function of the weight fraction of solid.

Microstructural Constituents

It was found that carbon additions from 0.03 to 0.11 wt. %, at 0.5 wt. % manganese and 7 wt. % nickel reduced austenite transformation temperature from 490 to 355 °C. In doing so, the microstructure became mainly martensitic (Figure 9) with some bainite also forming in dendrite core regions. Calculatating the martensite start temperature (M_S) and the bainite start temperature (B_S) using the empirical equations $M_S = 539 – 423(\%C) – 30.4(\%Mn) – 17.7(\%Ni) – 12.1(\%Cr) – 7.5(\%Mo)$ and $B_S = 830 – 270(\%C) – 90(\%Mn) – 37(\%Ni) – 70(\%Cr) – 83(\%Mo)$ [38–39] it is seen that the predicted B_S of the low carbon weld metal of 498 °C agrees very well with the measured transformation temperature of 490 °C. For the high carbon variant, the calculated M_S is 347 °C which is also close to the measured transformation temperature of 355 °C. Clearly, predicted and measured transformation temperatures are in good agreement with the observed dominant microstructural constituents.

In order to visualise the effect of alloying content on the M_S (Figure 20) and the B_S (Figure 21) temperatures plots were made using the M_S and the B_S equations [38–39] as a function of Mn and Ni content along with the base input composition of Table 2. It is shown in these diagrams that with greater alloying contents, both the martensite start temperature M_S and bainite start temperature B_S are suppressed to lower temperatures. As expected the spacing between the iso-M_S and iso-B_S lines are different. When the difference between the two temperatures is plotted as shown in Figure 22, it is found that Ms and B_S are approximately equal along a line passing through the alloying content of 2 wt % Mn and 7 wt % Ni. It can be seen from this diagram that reducing Mn or Ni is predicted to promote bainite while increasing Mn or Ni will promote the formation of martensite. Also plotted in Figures 20 – 22 is the variation in alloying content between interdendritic and dendrite core regions as measured using EDX (Table 4) for weld metals 7-2L250 and 7-0.5L250 along with the recorded transformation start temperature from dilatometry measurements (Table 5).

From dilatometry experiments, it was found that austenite transformation with weld metal 7-2L250 started in the region of 373 °C (Table 5). The microstructure was found to be a mixture of upper bainite along with a novel constituent with a large grain size in dendrite core regions while martensite was found at interdendritic regions (Figures 9, 10 and 12). From a detailed study of the novel constituent, it was characterised to be that of coalesced bainite. Coalesced bainite is believed to form when B_S and M_S are close to each other which is in agreement with the predictions using the empirical equations (Figure 22). A complete discussion about coalesced bainite may be found elsewhere [33] while the mechanism of how it forms is presented in Figure 23 along with those of upper and lower bainite. In short, coalesced bainite is believed to form when bainitic ferrite plates with identical orientation coalesce to form one big supersaturated plate.

The differences in microstructure across the dendrites in weld metal 7-2L250 may be explained in terms of the local composition measured with EDX (Table 4). Interdendritic regions which

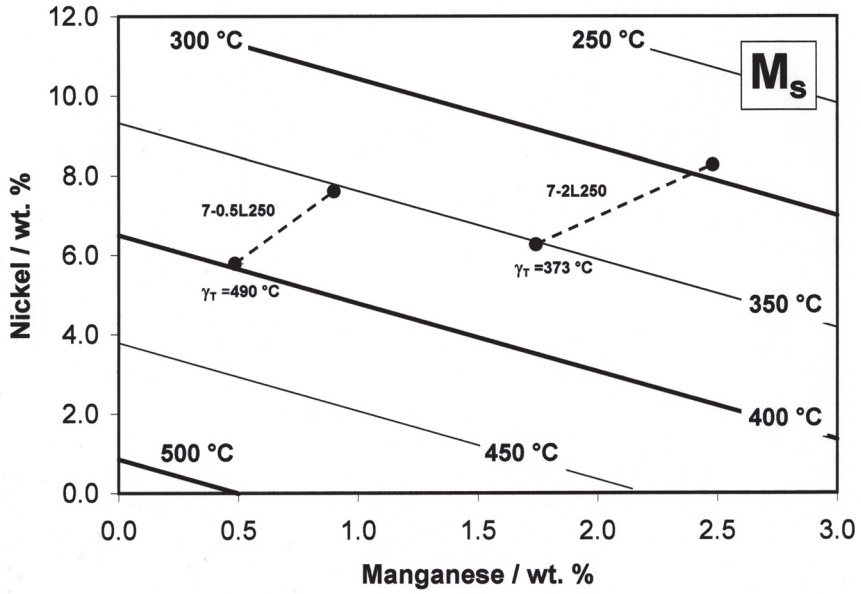

Figure 20 The martensite start temperature (M_S) as a function of Mn and Ni content calculated for the base composition in Table 2 using the M_S empirical equation [38]. Also plotted is the variation in alloying content between interdendritic (richer contents) and dendrite core regions (leaner contents) for 7-2L250 and 7-0.5L250. The austenite transformation temperatures (γ_T), recorded with dilatometry are also shown.

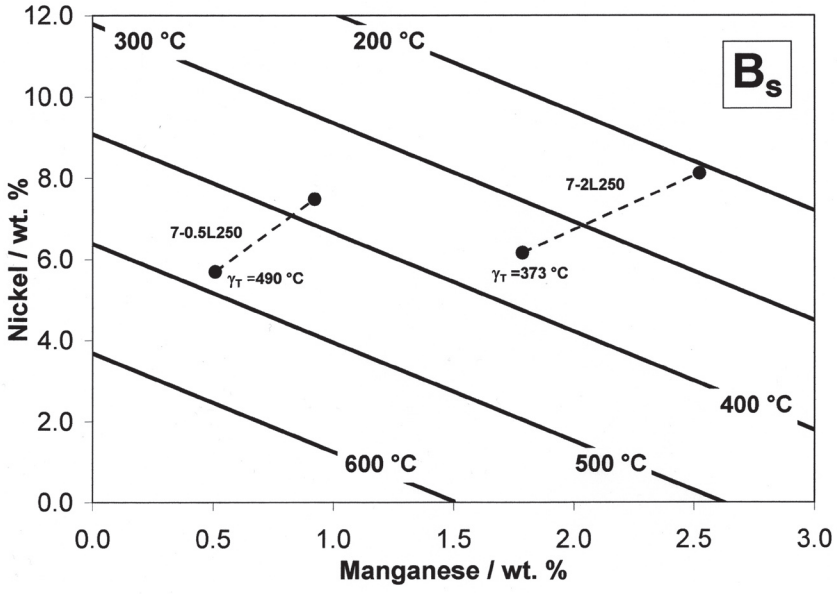

Figure 21 The bainite start temperature (B_S) as a function of Mn and Ni content calculated for the base composition in Table 2 using the B_S empirical equation [39]. The austenite transformation temperatures (γ_T), recorded with dilatometry specimens are shown for weld metals 7-2L250 and 7-0.5L250 along with the variation in alloying content between interdendritic (richer contents) and dendrite core regions (leaner content).

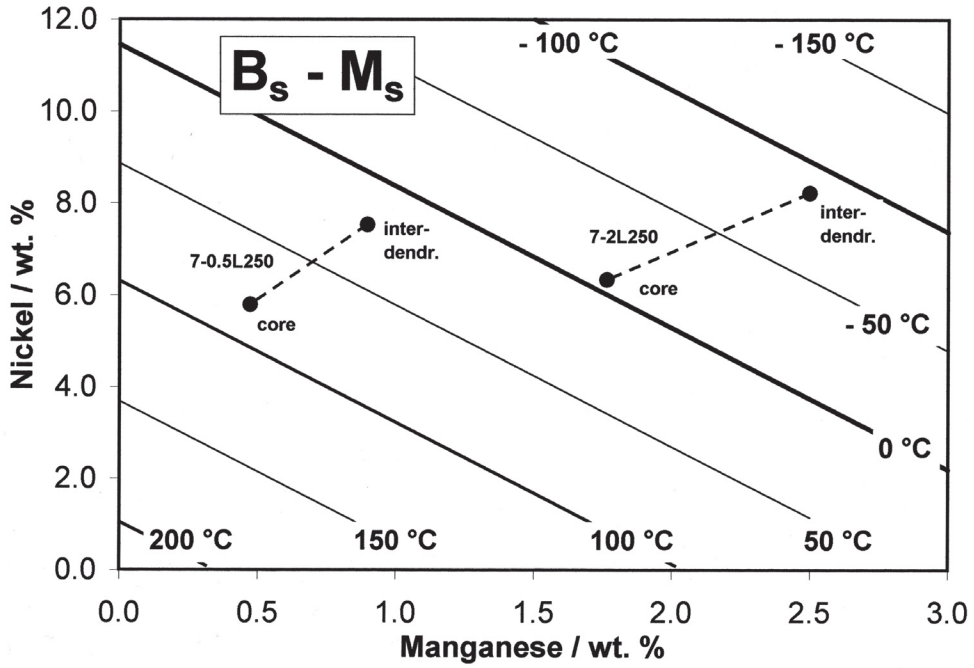

Figure 22 The difference between B_S and M_S as a function of Mn and Ni content calculated using the B_S and M_S empirical equations [38–39] along with the base composition in Table 2. A negative difference means martensite is more likely to form while a positive value means bainite is more likely to form. The compositional variations between interdendritic and dendrite core regions are illustrated for 7-0.5L250 and 7-2L250.

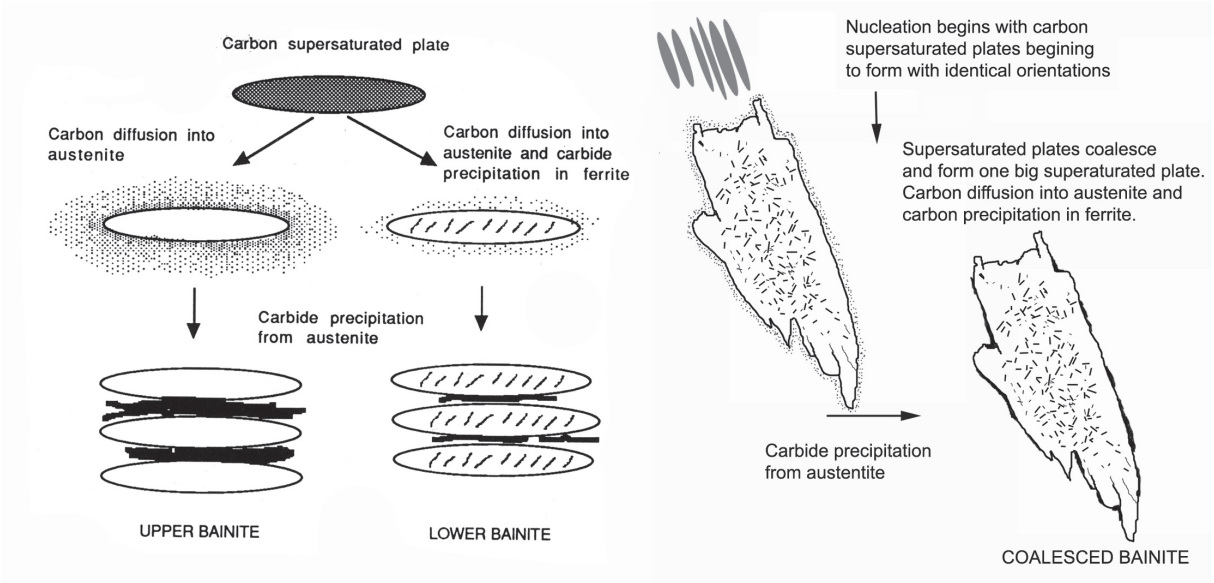

Figure 23 Schematic representation of the formation of upper and lower bainite [40] along with coalesced bainite [33].

were enriched in alloying content are believed to transform at lower temperatures predominantly to martensite. This is supported by the greater austenite stabilisation which is also in agreement with dilatometry experiments and predictions of B_S and M_S (Figures 20–22). Allowing for the effects of segregation and using the measured compositions in dendrite core regions (Table 4), it is found that there is good agreement between the observed and the calculated transformation temperatures.

Reducing manganese content with weld metal 7-0.5L250 was found to promote austenite transformation at a higher temperature (in the region of 490 °C, Table 5). In this weld metal the microstructure was that of mainly upper and lower bainite in dendrite core regions as shown in Figure 9, with some little martensite forming at interdendritic regions.

Finally based on microstructural observations, dilatometry experiments, M_S and B_S predictions and literature, a constitutional diagram was constructed showing the dominant microstructural constituents as a function of nickel and manganese content. In Figure 24 microstructural regions are shown together with the martensite composition start line taken from literature [41]. Also plotted is the line where B_S and M_S are equal. In conclusion, all microstructural observa-

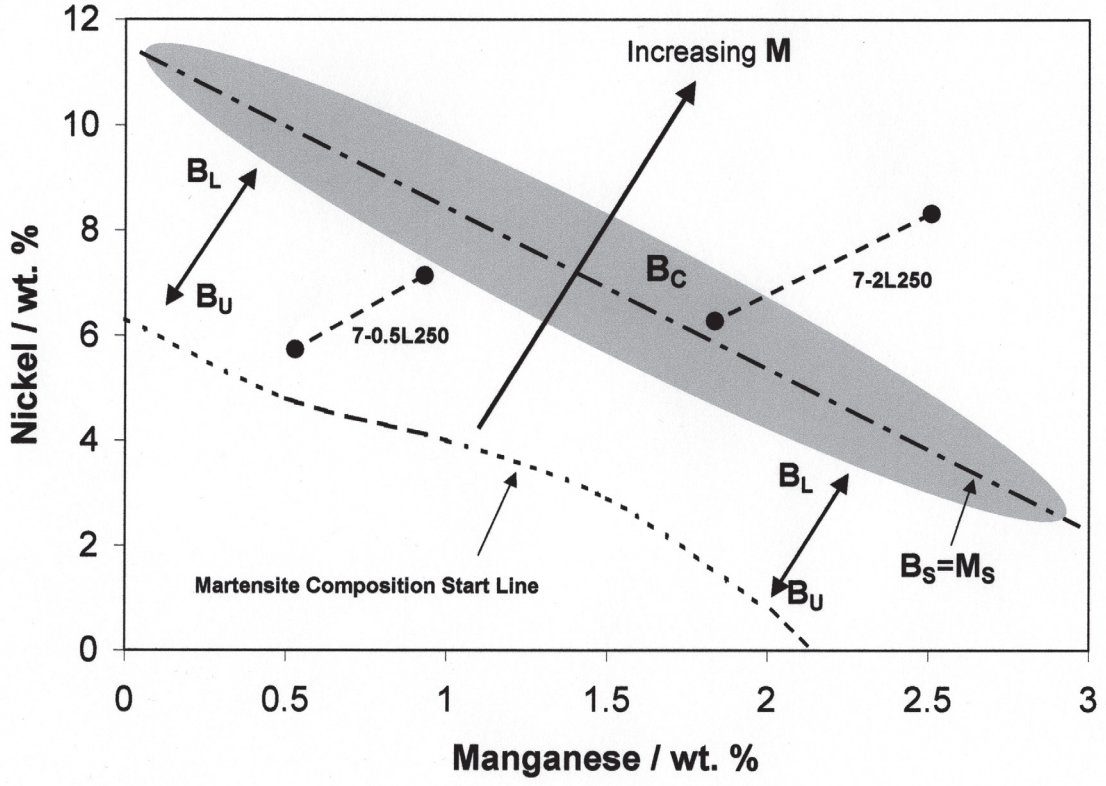

Figure 24 Constitutional diagram showing the dominant microstructure as a function of Ni and Mn content for the base composition 0.034 C, 0.25 Si, 0.5 Cr and 0.62 Mo. The martensite composition start line is taken from literature [41]. Also shown is the line where B_S and M_S are calculated to be equal using empirical equations [38–39].

tions for the 7 or 9 Ni weld metals, including effects of segregation are in excellent agreement with the proposed constitutional diagram. However it should be kept in mind when applying the diagram that effects of variation in cooling rate and changes in alloying elements other than Mn and Ni also have to be considered.

Transformation Behaviour on Tempering

Dilatometry experiments showed that changes in nickel, manganese and carbon content give a variation in Ac_1 and Ac_3 temperatures on reheating. With greater nickel content austenite formed earlier on reheating while reducing manganese was found to increase Ac_1 and Ac_3 to higher temperatures. Carbon additions with 7 wt. % Ni and 0.5 wt. % Mn were found to reduce Ac_1 slightly but had no effect on Ac_3. Although the changes in Ac_1 and Ac_3 are not that large, nevertheless they will have an effect on the relative amount of tempered microstructure within the welded joints as well as the degree of tempering. Lower Ac_1 and Ac_3 temperatures give greater amounts of stronger freshly formed microstructural constituents while higher Ac_1 and Ac_3 promote more tempering which is likely to give a tougher microstructure. Possible effects on strength and impact toughness will be discussed in Part B [31].

Conclusions

New development routes were explored to increase strength while maintaining impact toughness in high strength steel weld metals. Using neural network modelling it was predicted that reducing manganese concentrations at all Ni levels lead to a large increase of toughness and that nickel must be added in a controlled manner depending on manganese concentration in order to have a positive effect on toughness. Carbon additions were predicted to enhance yield strength at moderate expense to impact toughness.

Based on these predictions, experimental welds were made using SMAW with Mn at 0.5 or 2.0 wt. % and Ni at 7 or 9 wt. %. Additional welds were made where carbon was varied between 0.03 and 0.11 wt. % with Mn set at 0.5 wt % and Ni at 7 wt. %.

Based on Thermo-Calc modelling and observed segregation behaviour it was concluded that the weld metals solidified completely as austenite. Nickel and carbon additions were found to stabilise austenite to lower transformation temperature while manganese reductions promote the decomposition of austenite at higher temperatures. For a combination of high nickel and manganese a mixture of upper and coalesced bainite was found in dendrite core regions with mainly martensite present in interdendritic regions. A manganese reduction was found to reduce the amount of coalesced bainite and promote greater amounts of upper bainite within the microstructure while carbon additions were found to promote martensite.

A constitutional diagram has been constructed summarising the effects on microstructure of varying manganese and nickel contents.

In Part B of this work, the mechanical properties are presented and discussed in relation to the microstructure and the neural network predictions.

Acknowledgements

Prof. L.-E. Svensson of Chalmers University of Technology is thanked for fruitful discussions. K. Frisk and A. Markström of the Swedish Institute of Metals Research are thanked for producing Thermo-Calc predictions. ESAB AB is thanked for the production of experimental weld metals, permission to publish results and financial support. Knowledge Foundation of Sweden is thanked for additional financial support.

References

1. L.-E. Svensson: Svetsaren, 54, January (1999).
2. D.J. Widgery, L. Karlsson, M. Murugananth & E. Keehan, Approaches to the develop ment of high strength weld metals, Proceedings 2nd Int. Symposium on High Strength Steel, Norway (2002).
3. W.C. Leslie: The physical metallurgy of steels. (1981), London: McGraw - Hill.
4. A.C. Davies: Welding Science and Technology. 10 Ed. The Science & Practice of Welding. Vol. 1. (1992): Cambridge University Press.
5. ASM: Properties and Selection Iron, Steel and High Performance Alloys. 10 Ed. ASM Handbook. Vol. 1 (1990).
6. L.-E. Svensson: Control of microstructure and properties in steel arc welds, CRC Press, Inc., 1994
7. J.F. Deloach: Proceedings, International Conference on Welding Technology, Material and Fracture, (1990), Geesthacht, Germany: F-93460 Gournay-sur-Marne, France; IITT International; 1990.
8. P.R. Oldland, CW Ramsay, DK Matlock, DL Olson: Welding Journal, 68 (1989), April, p. 158.
9. M.G. Vassilaros, E.J. Czyryca: Proceedings, Advances in Low-Carbon High Strength Ferrous Alloys (LCFA-92), Jamshedpur (India), March 25–28, (1992): Key Engineer -ing Materials (Switzerland).
10. D.B. Fleming, A.Q. Bracarense, S. Liu, D.L. Olson: Welding Journal (USA), 75 (1996), June: p. 171s–183s.
11. D.E. McRobie, J.F. Knott, Material Science and Technology, 1 (1985), May: pp. 357 – 365.
12. L.-E. Svensson, B. Gretoft: Welding Journal, 69 (1990), December: p. 454.
13. T.W. Lau, M.M. Sadowsky, T.H. North, G.C. Weaterly: The Metallurgical Society / AIME, 1987 p. 349.
14. M. Lord: Design and modelling of ultra – High Strength Steel Weld Deposits, in

Materials Science and Metallurgy, (1999), University of Cambridge: Cambridge.
15. D.J. Abson, and R.J. Pargeter, 1986, Inter. Metal Rev., 31:141–194
16. O. Grong, D. K. Matlock, 1986, Inter. Metal Rev., 31: 27–48
17. R.A. Farrar and P.L. Harrison, 1987, J. Mater. Sci., 22:pp.239–244
18. D.S. Taylor and G.M Evans,1983, Metal Constr., 15: 438–443
19. G.M Evans, 1991, Joining Sciences, 1: pp. 2–13
20. P.L. Harrison and R.A. Farrar, 1987, Metal Constr. 19: pp. 392R–399R and 447R–450R
21. Wang W. and Liu S.: Welding Journal, July 2002, p. s–132.
22. J. Liao, H. Kametani, H. Okada and K. Ikeuchi, Toughness of weld metals of 950 MPa High Strength Steel, Proceedings of the 7th Int. Symposium., pp. 809–814, Japan Welding Society, 2001.
23. Y. Kang, H.J. Kim, and S.K. Hwang: ISIJ International (Japan), 40 December (2000), p. 1237.
24. Fairchild D.P., Macia M.L., Bangaru N.V. and Koo J.Y.: Proc. 13th Int. Offshore and Polar Eng. Conf., Honolulu, Hawaii, USA, May 25–30, 2003, p. 26.
25. Lord, M; Jennings, G; Effect of interpass temperature on properties of high strength weld metals, Svetsaren (Sweden), vol. 54, no. 1–2, pp. 53 – 58, 1999
26. D.J.C. Mackay: Neural Computation. (1992), p. 448.
27. D.J.C. Mackay: Neural Computation. (1992), p. 415.
28. H.K.D.H. Bhadeshia: ISIJ International (Japan), 39 (1999), October: p. 966–979.
29. M. Murugananth, H.K.D.H. Bhadeshia, E. Keehan, H.-O. Andrén, L. Karlsson: Proc. 6th Inter. Seminar, "Numerical Analysis of Weldability", Oct 1–3 (2001), Graz, Austria.
30. Murugananth Marimuthu, Design of welding alloys creep and toughness, (2002), Uni versity of Cambridge: Cambridge
31. E. Keehan, L. Karlsson, H.-O. Andrén, L.-E. Svensson, New developments with C–Mn–Ni high strength steel weld metals, Part B. Mechanical Properties, In Manuscript
32. SSAB Oxelösund, WeldCalc, Version 1.0.0, 98 – 99R.W.K.
33. E. Keehan, H. K. D. H. Bhadeshia, H.-O. Andrén, L. Karlsson, L.-E. Svensson, Micro structure characterisation of a high strength steel weld metal containing the novel con stituent coalesced bainite, In manuscript
34. E. Keehan, L. Karlsson, H.-O. Andrén, Influence of C, Mn and Ni contents on micro structure and properties of strong steel weld metals, Part I. Effect of nickel content, In manuscript
35. E. Keehan, L. Karlsson, H.-O. Andrén, H. K. D. H. Bhadeshia, Influence of C, Mn and Ni contents on microstructure and properties of strong steel weld metals, Part II. Impact toughness gain from manganese reductions, In manuscript
36. E. Keehan, L. Karlsson, H.-O. Andrén, H. K. D. H. Bhadeshia, Influence of C, Mn and Ni contents on microstructure and properties of strong steel weld metals, Part III.

Increased strength from carbon additions, In manuscript
37. B. Sundman, B. Jansson and J.-O. Andersson, Calphad, vol. 9, no. 2, pp. 153–190 (1985)
38. R.W.K. Honeycombe & H.K.D.K. Bhadeshia, Steel Microstructure and Properties, 2nd Ed., Edward Arnold, London, 1995, pp 103
39. R.W.K. Honeycombe & H.K.D.K. Bhadeshia, Steel Microstructure and Properties, 2nd Ed., Edward Arnold, London, 1995, pp 133
40. M. Takahashi, H.K.D.H. Bhadeshia, Materials Science and Technology, 6 (1990) 592 – 603.
41. Zhang Z, Farrar RA, Influence of Mn and Ni on the microstructure and toughness of C–Mn–Ni weld metals, Welding Journal 76 : (5) S183–S196 May1997